Solution Structure of PMP-D2, a 35-Residue Peptide Isolated from the Insect *Locusta migratoria*†

Georges Mer,*,‡ Christine Kellenberger,§ Patrice Koehl,‡ Roland Stote,|| Odile Sorokine,⊥ Alain Van Dorsselaer,⊥ Bang Luu,§ Hélène Hietter,§ and Jean-François Lefèvre‡

Ecole Supérieure de Biotechnologie de Strasbourg, UPR 9003 du CNRS, Bd Sébastien Brant, 67400 Illkirch-Graffenstaden, France, Laboratoire de chimie organique des substances naturelles, associé au CNRS, Université Louis Pasteur, 5 rue Blaise Pascal, 67084 Strasbourg, France, and Laboratoire de spectrométrie de masse bio-organique, associé au CNRS, Université Louis Pasteur, 1 rue Blaise Pascal, 67084 Strasbourg, France

Received July 8, 1994; Revised Manuscript Received October 7, 1994®

ABSTRACT: The three-dimensional solution structure of PMP-D2, a 35 amino acid peptide isolated from the insect *Locusta migratoria*, has been determined from two-dimensional ^{1}H NMR spectroscopy data. The structure calculations were performed from 222 NOE-derived interproton distances and 11 dihedral angles calculated from the $J_{HN-H\alpha}$ coupling constants, using either a combination of distance geometry and restrained simulated annealing or by restrained simulated annealing alone. PMP-D2 contains three disulfide bridges that have been assigned from NMR data and structure calculations and independently confirmed using chemical and enzymatic methods. The core region of PMP-D2 adopts a compact globular fold, stabilized by hydrophobic interactions, which consists of a short three-stranded antiparallel β-sheet involving residues 8−11, 15−19, and 25−29. Back-calculation of the NOESY spectra was used to validate the final structures. Analysis of the CD spectra of PMP-D2 under various conditions of ionic strength and in the presence of organic solvents demonstrates the high stability of this molecule. PMP-D2 was recently shown to inhibit Ca^{2+} currents. This activity is discussed based on the comparison of PMP-D2 three-dimensional structure with the recently established three-dimensional structure of the Ca^{2+} channel blocker ω-conotoxin GVIA.

Many of the peptides present in the central nervous system (CNS) of insects control development, reproduction, behavioral responses, and motility of muscles. A systematic study has been undertaken with the aim of characterizing the major peptides synthesized or stored in the CNS using *Locusta migratoria* as a model. From this investigation, several novel peptides have been isolated and sequenced (Hietter *et al.*, 1989−1991; Nakakura *et al.*, 1992). One of these molecules, referred to as PMP-D2, is a 35 amino acid peptide cross-linked by three disulfide bridges (Nakakura *et al.*, 1992). Although this peptide has been originally isolated from the brain of *L. migratoria*, it has also been found in the fat body and in the hemolymph of the same insect. The milligram quantities required to address the question of its biological activity cannot reasonably be extracted from insects and were thus obtained by solid-phase peptide synthesis (Kellenberger *et al.*, 1993). Recent work has established that synthetic PMP-D2 inhibits mammalian Ca^{2+} dependent currents at concentrations ranging between 0.1 and 10 μM (Harding *et al.*, 1994). Complementary biological tests are currently in progress to identify the Ca^{2+} channel subtype to which PMP-D2 binds and to understand the physiological role of PMP-D2 in *L. migratoria*. In parallel to the characterization of the biological activity of PMP-D2, the present study focuses on its three-dimensional structure, which has been determined in aqueous solution from two-dimensional ^{1}H NMR spectroscopy data and distance geometry or simulated annealing calculations.

MATERIALS AND METHODS

Peptide Preparation

The synthesis of PMP-D2 was performed manually, using a F_{moc} strategy, as described by Kellenberger *et al.* (1993). After synthesis, oxidative refolding of PMP-D2 was carried out by air oxidation at pH 8. The authenticity of synthetic PMP-D2 was assessed by electrospray mass spectrometry (ESMS),[1] amino acid analysis, and automated Edman degradation under the same conditions as described in Nakakura *et al.* (1992). Synthetic and natural peptide (isolated from the brain or the hemolymph) were co-injected onto a C_{18} RP-HPLC column [HPLC chromatograms were run as described in Nakakura *et al.* (1992)] and were found to co-elute.

Assignment of Disulfide Bonds by Chemical and Enzymatic Methods

Trypsin/AspN Endopeptidase. PMP-D2 (500 μg, 0.13 μmol) was incubated with trypsin (25 μg) in combination with AspN endoproteinase (3 μg) for 18 h at 37 °C in 0.5

† G.M. was supported by a CNRS région Alsace fellowship. C.K., B.L., and H.H. acknowledge the support by the EEC (Contract BIO2CT 930073).

* To whom correspondence should be addressed.
‡ Ecole Supérieure de Biotechnologie de Strasbourg.
§ Laboratoire de chimie organique des substances naturelles.
|| Laboratoire de chimie biophysique, ULP, Strasbourg.
⊥ Laboratoire de spectrométrie de masse bio-organique.

® Abstract published in *Advance ACS Abstracts,* November 15, 1994.

[1] Abbreviations: CD, circular dichroism; COSY, correlated spectroscopy; DSS, 2,2-dimethyl-2-silapentane-5-sulfonate; ESMS, electrospray mass spectrometry; HOHAHA, homonuclear Hartmann−Hahn; NMR, nuclear magnetic resonance; NOE, nuclear Overhauser enhancement; NOESY, NOE spectroscopy; rmsd, root mean square difference; PITC, phenyl isothiocyanate; RP-HPLC, reversed-phase high-performance liquid chromatography.

0006-2960/94/0433-15397$04.50/0

mL of 50 mM Tris-HCl buffer (pH 7.5) containing 1 mM iodoacetic acid (in order to minimize the potential disulfide scrambling during the enzymatic cleavage). The reaction mixture was directly loaded onto a C_{18} RP-HPLC column (300 Å, 250 mm × 4.6 mm; Vydac, Hesperia, CA) equilibrated with 0.1% trifluoroacetic acid and eluted with a linear gradient of 0−40% acetonitrile over 40 min at 1 mL/min; elution of the peptides was monitored at 214 nm. The major peaks were collected, dried in a Speed-Vac concentrator, and analyzed by ESMS; some of them were then submitted to automated Edman degradation.

Extraction of Peptide from Sequencer Membrane. After several cycles of Edman degradation, the peptide was extracted from the sequencer membrane with 80% (v/v) formic acid in water for 5 min at room temperature. The formic phase was filtered out using a ultrafree MC Millipore 10000 NMWE (to remove the silica), and the sample was concentrated up to 100 μL, diluted with water, and injected onto the HPLC column.

Partial reduction and alkylation were performed according to Gray (1993a,b). PMP-D2 (100 μg, 26 nmol) was incubated in 200 μL of a 10 mM TCEP [tris(2-carboxyethyl)-phosphine] solution in 90 mM citrate buffer (pH 3) for 12 min at 55 °C. The reaction was stopped by loading the reacting mixture onto a C_{18} RP-HPLC column, and the products were separated using a linear gradient of 0−40% acetonitrile over 40 min at a flow rate of 1 mL/min. In a first experiment, the collected peaks were identified by their retention time and ESMS analysis.

In a second experiment, the partially reduced peptide as collected in HPLC effluent (pH 2) was immediately alkylated by rapid mixing with 0.2 mL of 500 mM Tris-HCl buffer (pH 8) saturated with iodoacetamide (100 mg) for 20 s at room temperature. The reaction was stopped by the addition of 0.1 mL of trifluoroacetic acid, and again the products were separated using a linear gradient of 0−40% acetonitrile over 40 min at a flow rate of 1 mL/min. The collected peaks were identified by their retention time, ESMS analysis, and automated microsequencing.

Automated Microsequencing. Automated Edman degradation was performed on an Applied Biosystems sequencer, Model 473 A, in the liquid pulse mode.

Electrospray mass spectrometry (ESMS) was performed in the positive mode as described by Jaquinod *et al.* (1993) on a VG Bio-Q (Bio-Tech, Manchester, UK). The peptides were dissolved in H_2O/CH_3CN (50/50, v/v) with 1% acetic acid at a concentration of approximately 5−10 pmol/μL.

Circular Dichroism Analyses

CD spectra were obtained on an Aviv Model 62D spectropolarimeter at 25 °C, using 1-mm quartz cells. Data points were recorded between 260 and 180 nm, every 0.5 nm, with a time constant of 4 s and a spectral band width of 1.5 nm. Results are the average of three repetitive scans, corrected for solvent and cell contribution. Mean residue ellipticities are expressed in deg·cm^2·dmol^{-1} and were calculated based on the net peptide content as determined spectrophotometrically and from amino acid analysis. PMP-D2 was dissolved in bi-distilled water (pH 6.6), in the absence or presence of trifluoroethanol (27%, v/v), acetonitrile (27%), or NaCl (10, 50, 100, or 500 mM). To study the temperature dependence, CD spectra were run from 5 to 90 °C with 5 °C steps.

NMR

Experiments. All NMR spectra were recorded on a Bruker AMX-500 spectrometer. The peptide was dissolved in 400 μL of either D_2O or 90% H_2O/10% D_2O to give a final 3 mM concentration. Most experiments were done at pH 3 and 25 °C; however, to complement the data, spectra were also obtained at 35 and 45 °C and at pH 4.2. Spin system identification and sequential assignments were achieved using HOHAHA (Braunschweiler & Ernst, 1983; Bax & Davis, 1985), DQF-COSY (Rance *et al.*, 1983), and NOESY (Jeener *et al.*, 1979; Kumar *et al.*, 1980) experiments. In HOHAHA experiments, the proton magnetization was spin locked through 40- or 80-ms MLEV17 mixing sequences with a field strength of 8 kHz, flanked by 1.5-ms trim pulses. Six mixing times (from 50 to 300 ms) were used for NOESY in order to identify spin diffusion effects. All spectra were recorded with a sweep width of 6024 Hz and a relaxation delay of 3.5 s, during which time the solvent resonance was presaturated. The 2D data sets were typically 512 t_1 increments of 48 scans with 2048 real points except for the DQF-COSY spectra where 4096 real points were collected in order to increase the spectral resolution for the measurement of $^3J_{HN-H\alpha}$ coupling constants. Phase-sensitive detection along ω_1 was achieved using time-proportional phase incrementation (TPPI) of the initial pulse (Marion & Wüthrich, 1983).

Data Processing. The data were zero-filled and processed by apodization with a 60 or 90° shifted sine-squared bell window function in both dimensions before Fourier transform and baseline correction. The final size of the matrices was 2K × 1K real points (HOHAHA, NOESY) or 4K × 1K (DQF-COSY). Spectra processing was performed on an IBM RISC 6000 workstation using the software package FELIX (Version 2.05, from Biosym Inc.).

Experimental Constraints. NOESY cross-peak volumes were integrated from spectra recorded with a 100-ms mixing time, using the integration routine provided in FELIX. The distance constraint r_{ij} between two protons i and j was then estimated as follows (Wüthrich, 1986):

$$r_{ij} = r_{ref}\left(\frac{NOE_{ref}}{NOE_{ij}}\right)^{1/6} \quad (1)$$

where ref indicates a reference (taken to be the geminal β-protons distance, in which case r_{ref} = 1.8 Å), and NOE_{ref} and NOE_{ij} are the NOESY volumes for the ref and ij cross-peaks, respectively. Equation 1 is approximate since it does not take into account spin diffusion and internal motion. To account for these effects, distance constraints were classified into three categories corresponding to upper distance limits of 2.5, 3.5, and 5 Å rather than as strict constraints. Pseudoatom corrections were applied when stereospecific assignments were not available.

Slowly exchangeable amide protons were identified by measurement of the proton/deuterium exchange kinetics, leading to the introduction of 10 hydrogen bonds constraints (1.8 Å < d_{H-O} < 2.2 Å and 2.8 Å < d_{N-O} < 3.3 Å) in the calculations (see below).

Eleven dihedral ϕ angles were estimated from $^3J_{HN-H\alpha}$ coupling constants (Karplus, 1959; Bystrov, 1976; Pardi *et al.*, 1992) that were either obtained from 1D spectra or estimated by fitting cross sections of the HN−Hα cross-peaks in a DQF-COSY using a software developed by P.

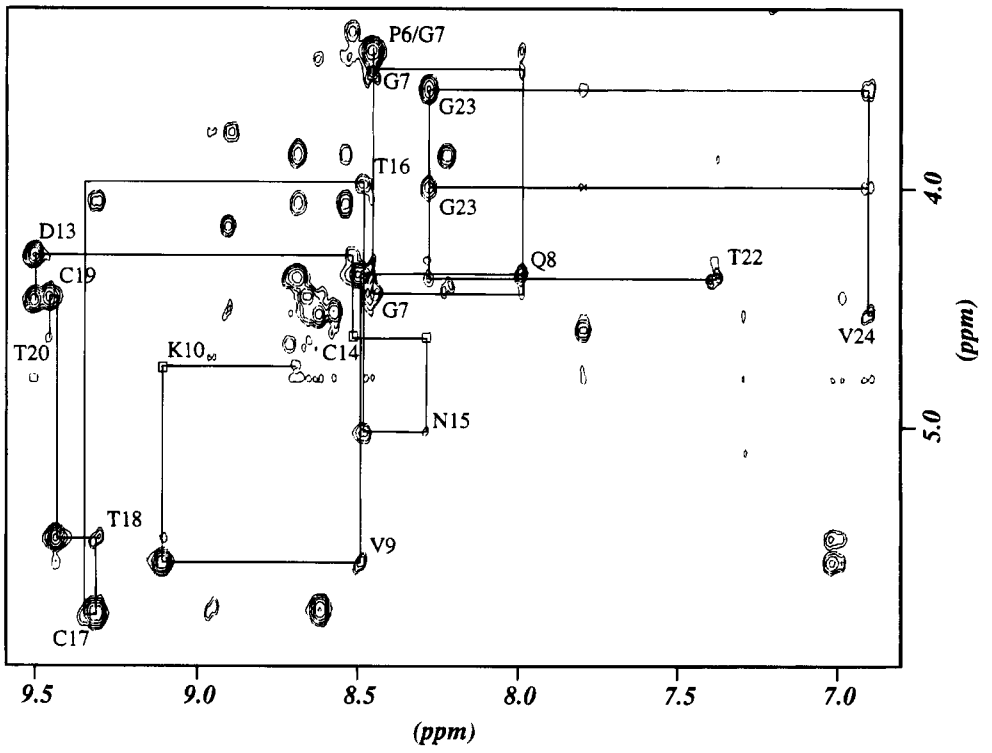

FIGURE 1: Fingerprint region of the 100 mM NOESY spectrum of PMP-D2 recorded at 298 K and pH 3. The sequential resonance assignments via $d_{\alpha}N(i,i+1)$ connectivities are illustrated for residues P6−K10, D13−T20, and T22−V24.

Koehl (unpublished results). The coupling constants were divided into small (J < 5.5 Hz), medium (8 Hz < J < 10 Hz), large (J > 10 Hz) and translated into dihedral angles respectively restrained to (−40 to −90°), (−80 to −160°), and (−100 to −140°) range.

Structure Calculations. The three-dimensional structure of PMP-D2 was calculated from the experimental distance and torsion angle constraints, either by simulated annealing or by a combination of distance geometry and simulated annealing. The simulated annealing protocol adopted, described in the X-PLOR 3.0 manual (Brünger, 1992), consists of four stages. First, a template structure with randomized backbone ϕ and ψ torsion angles is energy minimized over 50 iterations. The second stage involves 30 ps of high-temperature molecular dynamics at 1000 K. In the third stage, the system is progressively cooled to 300 K before a final conjugate gradient energy minimization of 200 iterations. Acceptable structures were further refined using the Charmm 22 potential energy function (Brooks *et al.*, 1983) by restrained steepest descent energy minimization of 1000 iterations.

Distance geometry calculations were performed in the dihedral angle space with the program Filman based on nonlinear Kalman filtering (Koehl *et al.*, 1992). In this procedure, the dihedral angles and their matrix of covariances are refined, leading to a final covariance matrix that provides estimates of errors on the dihedral angles. In order to restrain the conformational search, Filman calculations were first performed on two PMP-D2 segments corresponding to amino acids 4−10 and 11−35, respectively. The choice of these segments was dictated by PMP-D2 secondary structure (see Results). Dihedral angles of starting segments were generated randomly except for proline ϕ angles, which were set to −60°. When scalar coupling constants were available, the dihedral angles were generated randomly in their allowed regions. Initial variances on the dihedral angles were chosen so that two standard deviations correspond to half of the allowed range. When no dihedral angle constraints were available, the standard deviation was set to 60°. The ϕ angles of proline residues were fixed at −60°. The structures of each fragment were refined in 30 iteration steps, and their quality was evaluated on the basis of the average and maximum errors (Koehl *et al.*, 1992). For the whole structure calculations, starting structures were constructed using the backbone dihedral angles of the best segments and by random generation of the remaining dihedral angles. Initial variances were set as described above except for the backbone dihedral angles of the two fragments mentioned above which were constrained with a standard deviation of 5°. Acceptable structures obtained after 30 iteration steps were further refined through the simulated annealing procedure implemented in X-Plor before a final energy minimization using Charmm 22 as described previously.

NOE Back-Calculations. A theoretical NOESY map was calculated from the coordinates of each proton in the molecule by means of the relaxation matrix (Banks *et al.*, 1989) using a program developed by P. Koehl (unpublished results). For this calculation, an overall correlation time of 2 ns was assumed (rigid body approximation), which is consistent for a molecule of this size. Missing peaks in the reconstructed spectrum were used as a criterion to invalidate a structure.

RESULTS AND DISCUSSION

Spin System Identification and Sequential Assignment

The assignment of the proton resonances was straightforward. Most of the spin systems were identified on the basis of their amide protons chemical shifts by means of direct and relayed through-bond connectivities, using DQF-COSY and HOHAHA spectra. Sequential assignment was achieved by the identification of $d_{\alpha N}(i,i+1)$ or $d_{\beta N}(i,i+1)$ connectivi-

Table 1: ^{1}H Chemical Shifts of PMP-D2 in 90% H_2O (pH 3) at 298 K (ppm from DSS)[a]

	residue	NH	$C_\alpha H$	$C_\beta H$	$C_\gamma H$	$C_\delta H$	others
1	Glu		4.49	1.89; 2.04	2.34; 2.34		
2	Glu	8.90	4.51	2.09; 2.22	2.56; 2.56		
3	Lys	8.57	4.58	1.79; 1.74	1.99; 1.99	1.51; 1.57	ϵ-NH_3 7.52
							ϵ-CH_2 3.04
4	Cys	7.79	4.73	2.06; 2.55			
5	Thr	8.22	4.41	3.85	1.20		
6	Pro		3.42	1.81; 1.98	1.91; 2.07	3.61; 4.10	
7	Gly	8.45	3.50; 4.46				
8	Gln	7.99	4.35	2.23; 2.55	2.71; 2.71		δ-NH_2 7.85*; 7.02*
9	Val	8.49	5.56	1.98	0.96*; 1.07*		
10	Lys	9.11	4.73	1.37; 1.46	0.38; 0.51	0.73; 1.02	ϵ-NH_3 7.02
							ϵ-CH_2 1.11; 2.09
11	Gln	8.69	4.85	1.95; 2.04	2.37; 2.37		δ-NH_2 7.46*; 6.71*
12	Gln	8.45	4.46	1.66; 1.92	2.10; 2.10		δ-NH_2 6.65*; 7.36*
13	Asp	9.51	4.27	3.15*; 3.03*			
14	Cys	8.52	4.63	3.21; 3.34			
15	Asn	8.29	5.02	2.61; 2.90			γ-NH_2 7.93*; 7.65*
16	Thr	8.48	4.75	3.97	1.20		
17	Cys	9.35	5.78	2.80; 2.80			
18	Thr	9.31	5.46	4.04	1.17		
19	Cys	9.44	4.45	1.40; 3.05			
20	Thr	9.46	4.62	4.83	1.38		
21	Pro		4.29	1.91; 2.51	2.16; 2.01	4.00; 3.87	
22	Thr	7.38	4.37	4.50	1.19		
23	Gly	8.28	3.57; 3.98				
24	Val	6.90	4.52	2.09	0.86*; 0.68*		
25	Trp	8.62	4.74	3.01*; 3.18*			H2 7.29 H4 6.97
							H5 7.02 H6 6.90
							H7 7.47 NH 10.04
26	Gly	8.89	3.75; 4.70				
27	Cys	8.95	5.76	2.93*; 3.06*			
28	Thr	8.61	4.45	4.52	1.40		
29	Arg	8.66	4.65	1.99; 1.99	1.56; 1.62	3.22; 3.22	NH 6.71. 7.19
30	Lys	8.71	4.37	1.82; 1.82	1.71; 1.71	1.49; 1.49	ϵ-NH_3 7.56
							ϵ-CH_2 3.01
31	Gly	8.68	3.85; 4.06				
32	Cys	8.54	4.83	2.89; 3.45			
33	Gln	8.62	4.66	1.98; 2.12	2.42; 2.42		δ-NH_2 6.89; 7.57
34	Pro		4.42	1.96; 2.30	2.03; 2.03	3.68; 3.82	
35	Ala	8.46	4.32	1.43			

[a] (*) indicates stereospecific assignment; the first number is the shift of the proton or methyl group with the lower branch number.

ties. Strong $d_{\alpha P\delta}(i,i+1)$ NOEs were observed for all three proline residues, which indicates a trans conformation of the peptide bonds (Wüthrich, 1986). An example of NOESY spectrum illustrating the sequential assignment is shown in Figure 1.

Stereospecific assignment of β-methylene protons was obtained for some residues from a combination of the χ^1 angle coupling constant and distances between the β-methylene protons and the intraresidue amide proton (Wagner *et al.*, 1987). Side-chain amide protons of Asn and Gln residues were stereospecifically assigned by comparison of the intraresidual NOEs between the side-chain amide protons and the β- or γ-methylene protons resonances, respectively (Montelione *et al.*, 1984). The ^{1}H chemical shifts are given in Table 1.

Disulfide Bonding

In peptides containing tightly clustered disulfides, the assignment of the disulfide pairing is usually extremely difficult, due to the lack of techniques for cleaving the peptide chain between adjacent or closely spaced cysteines. Very often, chemical analysis or NMR analysis alone do not provide a complete and unambiguous identification of the disulfide linkage pattern, and only a combination of both methods enables the assignment of the disulfide pairing (Adler *et al.*, 1993). In the case of PMP-D2, the cysteine pairing was first identified using NMR and structure calculations and independently confirmed by chemical and enzymatic methods.

Identification of Disulfide Bridges from NMR and Structure Calculations. PMP-D2 contains six cysteine residues (Cys-4, -14, -17, -19, -27, and -32) which combine to form three disulfide bridges as determined by mass spectrometry analysis. Only one disulfide bond, between Cys-14 and Cys-32, was identified from NOEs between the β-methylene protons of these two cysteines. NOEs were also observed between β-methylene resonances of the four other cysteines but could not be used unambiguously to assign disulfide bonds.

In order not to bias the structure determination and to see whether the structure determination could confirm the disulfide bridge identified from NMR, initial X-Plor calculations were performed using only distance and dihedral angle constraints. No specific disulfide constraints were introduced. The lowest energy structures obtained were consistent with the disulfide bridge Cys14−Cys32, but it was not possible to unambiguously identify the two other bridges. Assuming that a disulfide bond between Cys-17 and Cys-19 could be ruled out on the basis of steric considerations, two hypotheses for the cysteine pairing were considered: Cys4−Cys17, Cys19−Cys27, Cys14−Cys32 or Cys4−Cys19, Cys17−Cys27, Cys14−Cys32. In order to assign

Table 2: Disulfide Bridges Identification

	[4−19, 17−27, 14−32]	[4−17, 19−27, 14−32]
	Average Number of NOE Distance Violations[a]	
<0.3 Å	7.3	29.7
<0.5 Å	2.5	18.1
	Number of Structures with Not More Than Two NOE Distance Violations[a]	
<0.3 Å	12	0
<0.5 Å	81	0

[a] 100 calculations in each case.

the complete cysteine pairing in PMP-D2, two other rounds of X-Plor calculations were performed using the NMR-derived distance and dihedral angle constraints as well as additional distance constraints respectively associated with one of the above sets of disulfide bridges. The average number of NOE distance violations for two sets of 100 structures corresponding to the two hypotheses as well as the number of structures with not more than two NOE violations, are reported in Table 2. The most likely pairings, according to these calculations, correspond to the second hypothesis, (i.e., 4−19, 17−27, and 14−32). In the case of the first hypothesis, all the calculated structures have NOE distance violations greater than 0.5 Å. This assignment was further confirmed by chemical and enzymatic methods (see below).

Determination of Disulfide Pairing by Chemical and Enzymatic Methods. In the case of PMP-D2, enzymatic cleavages alone failed to break the peptide into fragments. Consequently, enzymatic cleavages followed by several Edman degradation cycles were performed and yielded one disulfide. The two remaining bridges were determined by an alternative strategy, i.e., a partial reduction of the disulfides and their alkylation in conditions where scrambling is largely suppressed (Gray, 1993a,b).

The incubation of PMP-D2 with trypsin and AspN endoproteinase simultaneously yielded three major peaks, referred to as I, II, and III; by ESMS, peak I was shown to be intact PMP-D2 (observed mass = 3753.31, calculated mass = 3753.29), peak II was assigned as PMP-D2 with two cleavages in the peptidic backbone (observed mass = 3789.05 which corresponds to 3753 + 2 × 18 = 3789), and peak III was identified as PMP-D2 with one cleavage (observed mass = 3770.71 which corresponds to 3753 + 18 = 3771). The cleavage sites in peak II were localized by submitting peak II (approximately half of it) to Edman degradation; after one cycle of degradation, three residues were identified (namely, Glu, Asp, and Lys), after the second cycle, Glu and Gly, and after the third cycle, Lys and Asn. This indicated that the cleavage sites are localized at the N terminus of Asp-13 and at the C terminus of Arg-29. This experiment enabled us to exclude the existence of the Cys4−Cys32 linkage.

The remaining (second half) of peak II was subjected to three successive Edman degradation cycles, extracted from the sequencer membrane with 80% formic acid, purified by RP-HPLC, and analyzed by ESMS, which yielded a mass of 2604.9; this mass corresponds to the two fragments **C**(4)-TPGQVKQQ (calculated mass = 988.14) and T**C**(17)-T**C**(19)TPTGVWG**C**(27)TR (calculated mass = 1485.73) linked together: 988.14 + 1485.73 = 2473.87 − 4 = 2469.87 for two disulfide bridges (one disulfide between the two fragments, the other one between the two remaining Cys in the second fragment) + 135 = 2604.87 (observed mass = 2604.9) for the derivatization by PITC (phenyl isothiocyanate) of the ϵ-NH_2 of Lys-10 (the derivatization by PITC occurred during Edman degradation). From this experiment, it was concluded that Cys-14 and Cys-32 are connected by a disulfide bridge. To locate the two remaining disulfides,

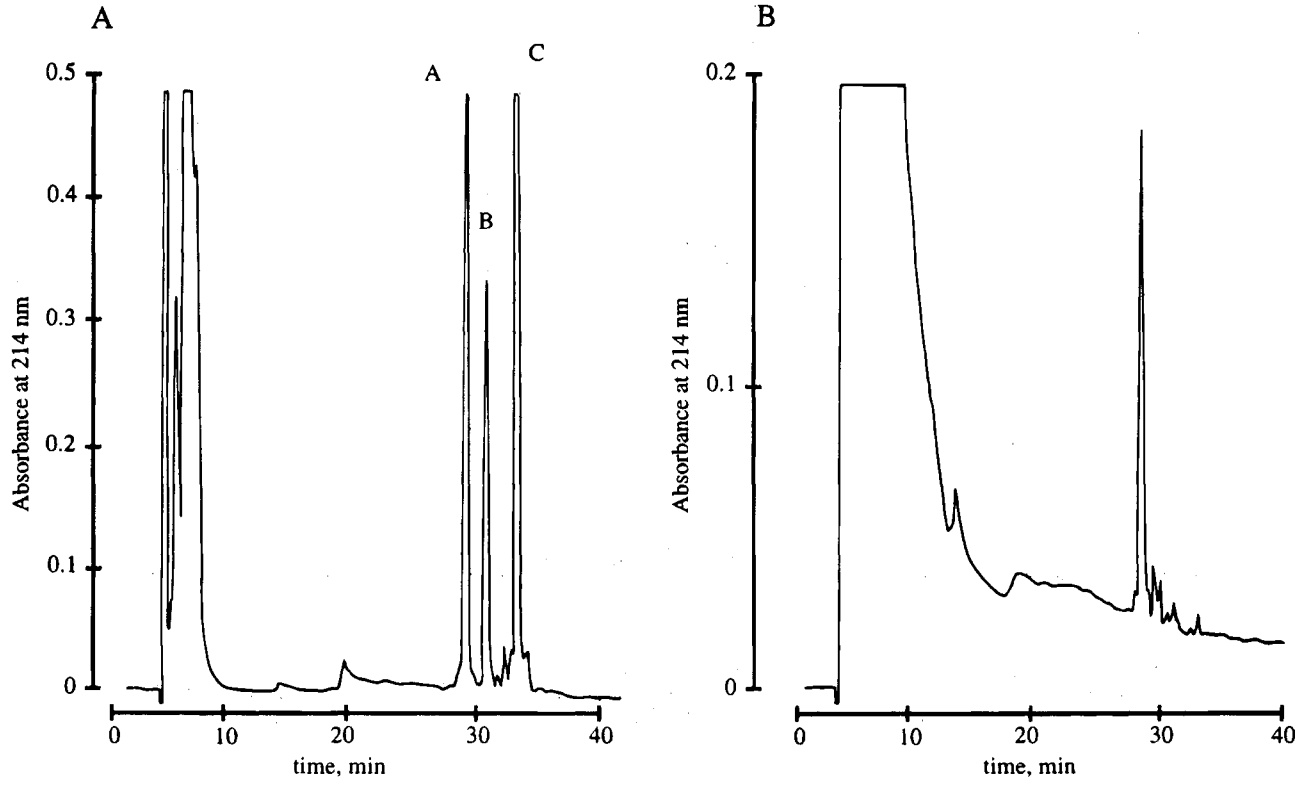

FIGURE 2: RP-HPLC chromatograms of PMP-D2 after partial reduction with tris(2-carboxyethyl)phosphine (A) and after alkylation of peak B (two disulfides reduced) (B) on a C18 Vydac column. The elution was performed with a linear gradient over 40 min from 0 to 40% acetonitrile in 0.1% trifluoroacetic acid at a 1 mL/min flow rate. Absorbance was monitored at 214 nm.

the partial reduction and alkylation method as described by Gray (1993a,b) was used. The reduction of PMP-D2 with the water-soluble tris(2-carboxyethyl)phosphine at pH 3 yielded three major products (Figure 2A) that were identified by ESMS; compound A was identified as unreacted PMP-D2, compound B was identified as partially reduced PMP-D2 (2 disulfides are reduced), compound C was identified as PMP-D2 completely reduced (3 disulfides reduced). In a second experiment, compound B was immediately alkylated by iodoacetamide in the conditions described by Gray (1993), which largely suppress the scrambling of the disulfides. After separation on RP-HPLC (Figure 2B), the major peak was dried in a Speed-Vac concentrator, and part of it was analyzed by ESMS (measured mass = 3984.96, which corresponds to 3756.76 + 4 × 57 = 3984.76), which indicated that among six Cys four were alkylated. To locate these four alkylated Cys, this peak was submitted to automated microsequencing, which showed that at the 4th and 19th cycle no amino acid could be detected as expected for a cysteine/cystine and that at the 14th, 17th, 27th, and 32nd cycle alkylated cysteine residues were detected. This enabled us to conclude that Cys-4 and Cys-19 are cross-linked by a disulfide bridge and since the Cys14-Cys32 linkage had been previously demonstrated (see above, trypsin/AspN endoproteinase), the Cys17-Cys27 pairing was deduced. Thus, we have obtained an unambiguous location of the disulfides, between Cys4−Cys19, Cys14−Cys32, and Cys17−Cys27.

Secondary Structure Elements

Data summarized in Figure 3 show that PMP-D2 essentially exhibits a β-type structure. The observed sequential and medium-range NOE connectivities between protons show no evidence for any α-helical secondary structure in PMP-D2. This is compatible with the absence of sequential amino acids having small $^3J_{HN-H\alpha}$ coupling constants. The off-diagonal correlations observed in the distance plot are consistent with a three-strand antiparallel β-sheet having a +1,+1 topology (Richardson *et al.*, 1981), expanding from Gln-8 to Arg-29 and including two loops centered on residues 13 and 22, respectively. This antiparallel β-sheet is further confirmed by large $^3J_{HN-H\alpha}$ values and by the slow exchange rate of amide protons expected to be involved in hydrogen bonds. The slow exchange rate of Val-9 amide proton cannot be explained from the β-sheet structure; this proton could be involved in a hydrogen bond with the side-chain carbonyl oxygen of Qln-8. The analysis of the α-protons chemical shifts (Wishart *et al.*, 1992) is also compatible with the three-strand antiparallel β-sheet. Analysis of short- and medium-range NOEs indicates that residues Thr-5 to Qln-8 form a canonical type-II β-turn with a proline (Pro-6) in position 2 and a glycine (Gly-7) in position 3. The secondary structure elements are shown in Figure 4A.

Three-Dimensional Structure

Distance Constraints. Analysis of the NOESY spectra led to the identification of 212 interresidue NOEs corresponding to 93 sequential, 22 nonsequential backbone/backbone, 53 nonsequential side-chain/backbone, and 44 non-sequential side-chain/side-chain connectivities. Combining the identification of slowly exchanging amide protons with the analysis of the secondary structure led to the determination of 20 additional distance constraints corresponding to 10 hydrogen bonds (see above).

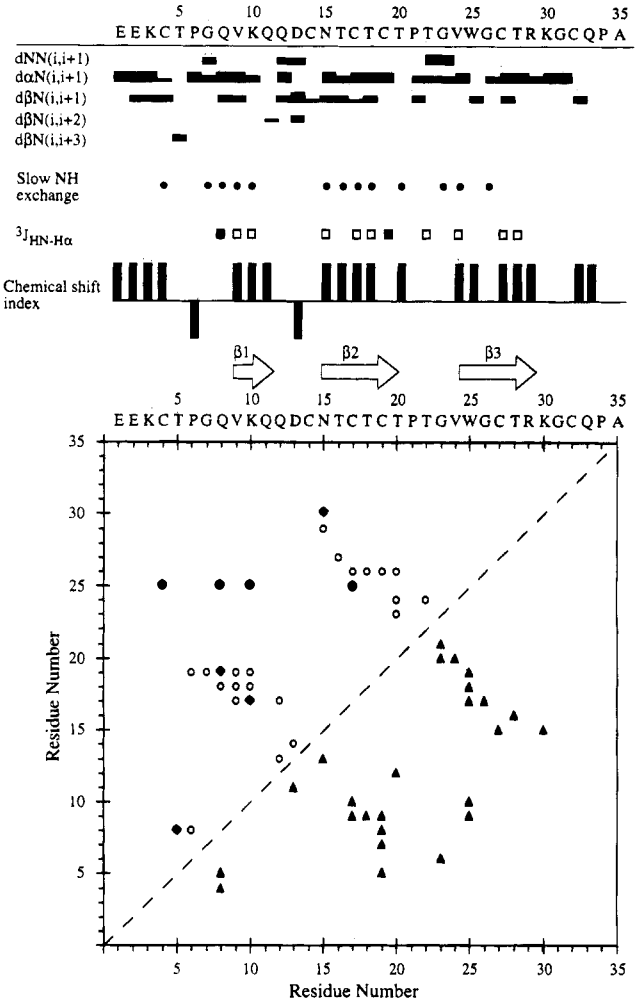

FIGURE 3: Summary of the NMR data used for the identification of secondary structure elements in PMP-D2. The sequential connectivities have been observed on a 100-ms NOESY spectrum recorded at 298 K and pH 3. The widths of the bars indicate the intensities of the corresponding NOEs, categorized as strong, medium, and weak. The closed circles represent the slowly exchanging amide protons, which have a lifetime longer than 2 h in a H_2O/D_2O exchange experiment at 298 K and pH 3. Small $^3J_{NH-H\alpha}$ coupling constants (lower than 6 Hz) are labeled with closed squares, while large $^3J_{NH-H\alpha}$ coupling constants (higher than 8 Hz) are labeled with open squares. The chemical shift index is calculated according to the method proposed by Wishart *et al.* (1992). Medium- and long-range NOEs are represented on the distance plot. The open circles indicate NOEs between backbone protons, the filled triangles indicate NOEs between backbone and side-chain protons, and the filled rectangles indicate NOEs between side-chain protons. The three strands of the β-sheet deduced from the experimental observations are represented in the middle of the figure.

Converged Structures. The structural statistics for the 10 best X-Plor structures as well as the energy terms calculated after Charmm 22 constrained energy minimization are given in Table 3. These structures satisfy the experimental constraints within acceptable limits and demonstrate good covalent geometry. They do not present any NOE-deduced distance violation greater than 0.5 Å nor any dihedral angle violation greater than 5°. Deviations from idealized covalent geometry are very small as judged by the low average rmsd (± standard deviation) values for the bond lengths (0.0063 ± 0.0005 Å) and for the angles (0.90 ± 0.14 Å).

Figure 4B illustrates the global fold of PMP-D2, and a stereoview of the best fit superposition of the 10 structures upon the mean coordinate positions between residues 4 and

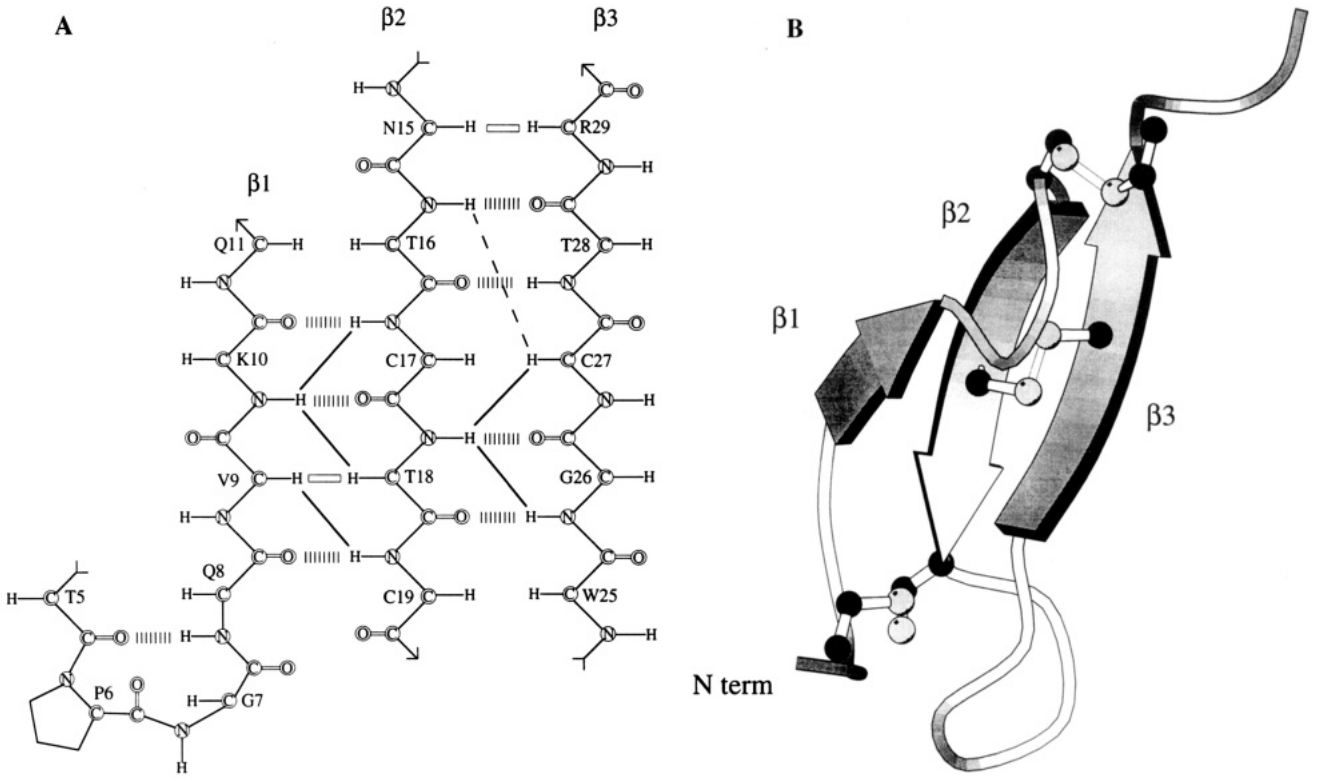

FIGURE 4: (A) Schematic representation of the secondary structure of PMP-D2. The interstrand NOEs are indicated by solid lines and the open bars indicate Hα−Hα connectivities. The hydrogen bonds deduced from slowly exchanging amide protons are represented by dashed lines. (B) Richardson (1981) diagram illustrating the tertiary fold of PMP-D2. The three strands of the β-sheet are labeled β1, β2, and β3. The side chains of the disulfide bonded cysteines are shown in 'ball and stick' form. This diagram was generated using the program Molscript (Kraulis, 1991).

Table 3: Structural and Energetic Statistics

(A) Compatibility with Experimental Constraints[a]	>0.1 Å	>0.2 Å	>0.3 Å	>0.4 Å
short (2−2.5 Å)	1.7	0.2	0	0
medium (2−3.5 Å)	14.8	7.5	1.0	0
long (2−5.0 Å)	16.5	4.1	1.0	0.4

(B) Stereochemistry and Energetics	
Root Mean Square Deviations from Idealized Covalent Geometry	
bonds (Å)	0.0063 ± 0.0005
angles (°)	0.901 ± 0.135
impropers (°)	0.701 ± 0.179
Residual Energies of Target Function Containing Repel Potential (kcal mol^{-1})	
E_{NOE}[b]	39.6 ± 2.7
E_{tors}[b]	1.0 ± 0.7
Average Energies Computed with Charmm 22 Force Field (kcal mol^{-1})[c]	
total energy	−1031.2
Lennard−Jones van der Waals energy	−184.4

[a] Average number of violations per structure. [b] The residual energies of the NOE (E_{NOE}) and dihedral torsion angle (E_{tors}) constraints are calculated with force constants of 50 kcal.mol^{-1} and 200 kcal.mol^{-1}.rad^{-2}, respectively. [c] These values have been obtained after restrained energy minimization using Charmm 22.

28 is shown in Figure 5. The well-defined part of PMP-D2 backbone adopts a compact globular fold, which forms a cavity demarcated by a three-stranded β-sheet with a right-handed twist [residues 8−11 (strand β1), 15−19 (strand β2), 25−29 (strand β3)] and by two irregular loops, involving residues 11−14 and 19−24 respectively. The loop, involving residues 5−8, is anchored to the β-sheet via the Cys4−Cys19 disulfide bridge. The average rmsd in atomic positions, calculated between the 10 structures for residues 4−28, is 0.72 ± 0.12 Å for the backbone atoms (N, C^{α}, C and O), and the rmsd including all the heavy atoms is 1.27 ± 0.22 Å.

Structure calculations of peptides based on NMR data usually raise two important questions: is there a unique fold of the peptide that can account for the experimental data, and how accurately is(are) this(these) fold(s) determined. In the case of PMP-D2, all reasonable structures (in terms of constraint violations) obtained either by simulated annealing using X-Plor or by distance geometry using Filman converged to the same fold, which confirmed the secondary structure assignment presented above. Illustration of the quality of the converged fold for the structure is usually provided by a superposition of the N best structures, as well as by a measure of the average rmsd among these structures. This procedure has the drawback of requiring an estimate of N that will correctly describe the sets that statistically verify the data. Another approach is to directly provide an estimate of the accuracy of the variables used in the structure calculation. Such a procedure was implemented for distance geometry in dihedral angle space in the program Filman based on optimal filtering. In Figure 6, an estimate of the errors on the angles ϕ and ψ obtained from Filman calculations is compared to the rmsd from the average structure calculated for the backbone atoms of each residue in the 10 structures; as is often the case, N and C terminal ends of the peptide are less constrained than the rest of the molecule. If we exclude N and C terminal ends, the loop between residues 11 and 14 is the less structurally defined region of the molecule, and it should be noted that in most of the structures Gln-12 or Asp-13 have positive ϕ angles. When the structures are matched to the residues 4−10 and 15−28, the rmsd (from the average) is 0.30 ± 0.05 Å for

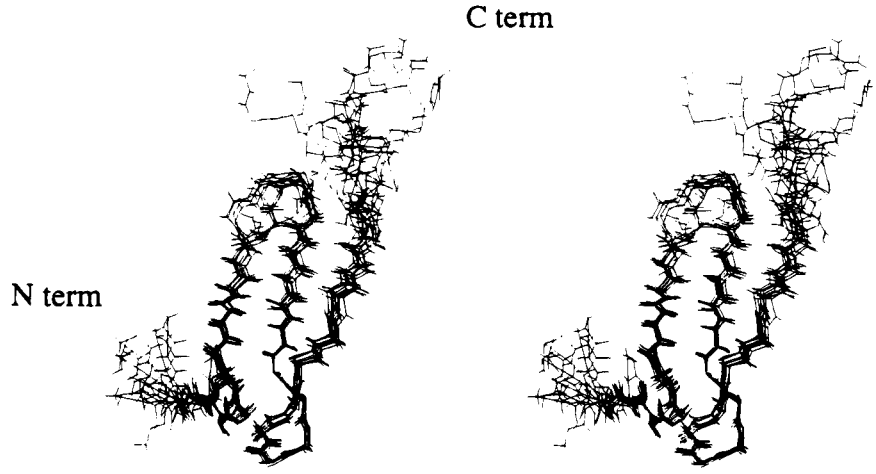

FIGURE 5: Stereoview of the backbone of the 10 best structures of PMP-D2 superimposed so as to minimize the rmsd from the mean structure for residues 4−28.

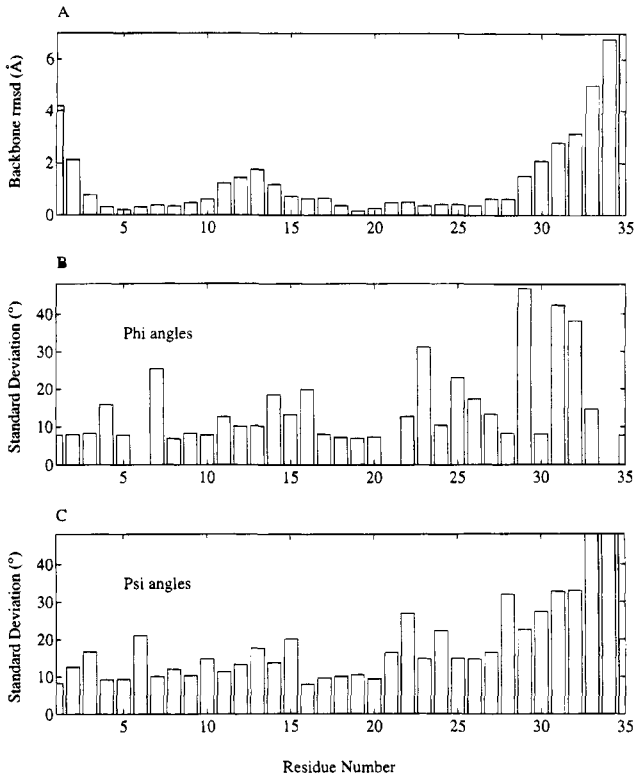

FIGURE 6: (A) rmsd of the backbone atoms calculated as a function of the residue number for the 10 best structures of PMP-D2 superimposed so as to minimize the rmsd from the mean structure for residues 4−28. Standard deviations on ϕ (B) and ψ (C) angles obtained from Filman calculations.

the backbone atoms and 0.55 ± 0.15 Å for the heavy atoms.

Visual comparison of experimental and back-calculated NOESY spectra has been used as an additional checkup of the structures. There was a good agreement between the calculated and experimental spectra for the 10 selected structures (data not shown). Some extra cross-peaks were found in all the reconstructed spectra, but this was not a criterion to invalidate a structure since the rigid model used for back-calculations does not take the effect of fast internal motions into account. On the contrary, a structure was rejected if cross-peaks were missing in the reconstructed spectrum.

Side Chain Organization. The average rmsd from the mean structure calculated for each residue clearly indicates that the best defined side chains are localized in the β-sheet

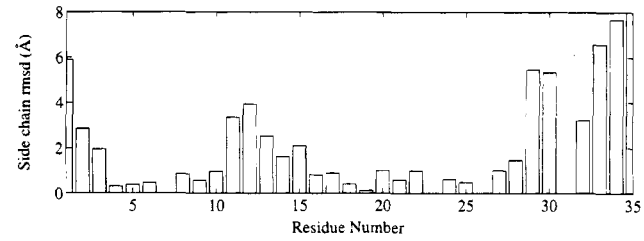

FIGURE 7: rmsd of the side-chain atoms calculated as a function of the residue number for the 10 best structures of PMP-D2 superimposed so as to minimize the rmsd from the mean structure for residues 4−28.

region of PMP-D2 (Figure 7). Most of them are involved in hydrophobic clusters. Thirty-six side-chain/side-chain NOEs have been found between residues that are inside the cavity (i.e., Cys-4, Cys-17, Cys-19, Trp-25, and Cys-27) or at the interface between the cavity and the solvent (i.e., Gln-8 and Lys-10). In this cluster, the aromatic ring of Trp-25 interacts strongly with the aliphatic part of Lys-10 (Figure 8); 21 NOEs have been identified between the side chains of Lys-10 and Trp-25. The Lys-10 side chain is in intermediate equilibrium between multiple conformations on the NMR chemical shift time scale as can be deduced from the broadening of its γ- and δ-methylene protons resonances (data not shown). Interestingly, PMP-D2 adopts a zipper-like arrangement due to the clustering of valines and threonines on the convex side of the β-sheet as shown in Figure 9. The clustering of these residues could be involved in the folding pathway of PMP-D2 as described by the "hydrophobic zipper" model of protein folding (Dill *et al.*, 1993). Three of these clusters (i.e., Val-9/Thr-18, Thr-16/Thr-28, and Thr-20/Val-24) have been identified by the presence of side-chain/main-chain NOEs in each case. An additional cluster involving Thr-5 and Thr-22 is observed in the three-dimensional structure; however, no NOE could be observed between the two residues. It should be mentioned that it was not possible to unambiguously identify methyl/methyl NOEs because of overlaps in the corresponding region of the spectrum.

Precise determination of disulfide bridge conformation in proteins appears to be a difficult problem as judged by the great number of molecules found to have disulfides built into distorted conformations (Morris *et al.*, 1992). In the case of PMP-D2, the disulfide bridge Cys4−Cys19 is well-defined, but its conformation is distorted with a χ^3 average

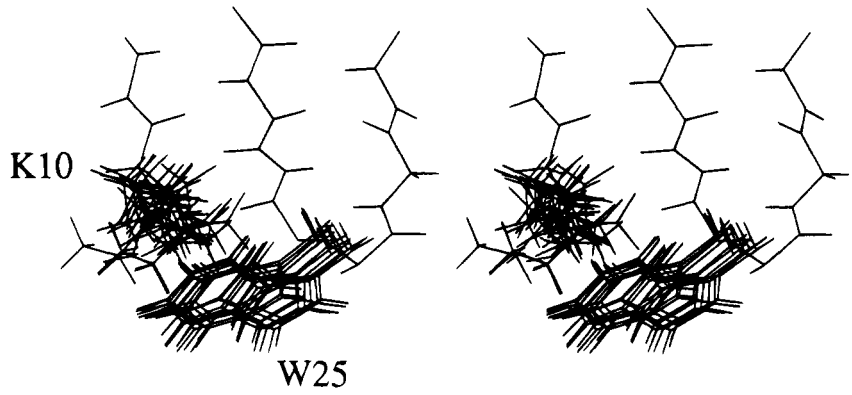

FIGURE 8: Stereoview of the interaction between W25 and K10 side chains for the 10 best structures. The structures have been superimposed so as to minimize the backbone rmsd from the mean structure for residues 4−28. Only the backbone of the mean structure has been represented for clarity.

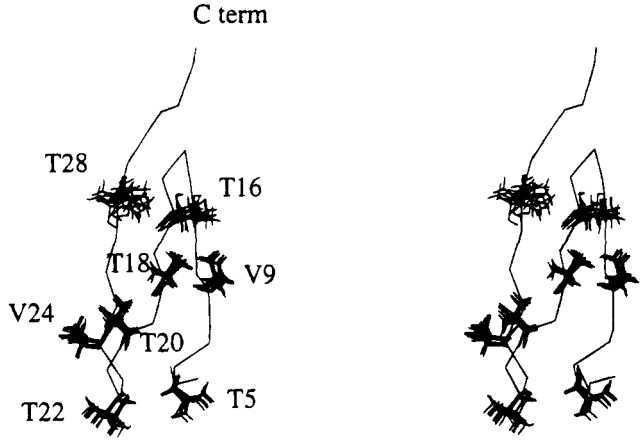

FIGURE 9: Stereoview of the distribution of threonine and valine side chains for the 10 best structures. The structures have been superimposed so as to minimize the backbone rmsd from the mean structure for residues 4−28. Only the backbone of the mean structure has been represented for clarity.

value of −66.3°. The disulfide bridge Cys17−Cys27 adopts from one structure to the other, either a right- or left-handed conformation (Thornton *et al.*, 1981) corresponding to opposite χ^3 average values of +76.1° and −90.6°, respectively. The conformation of Cys14−Cys32, which connects two poorly defined parts of the molecule (i.e., the 11−14 loop and the C terminal end), could not be characterized.

Stability of PMP-D2 Tertiary Structure

In order to investigate the stability of PMP-D2, we have examined the CD spectrum of the molecule under various conditions of ionic strength and in the presence or absence of trifluoroethanol or acetonitrile. The temperature dependence of the CD spectrum was also studied. The far-UV CD spectrum of PMP-D2 in water (pH 6.6) is characterized by a broad positive band at 227 nm of magnitude 4036 deg.cm^2.dmol and a strong negative band at 200 nm of magnitude 7930 deg.cm^2.dmol (Figure 10A). Therefore, the presence of an α-helical structure can be excluded. In addition, the absence of both a minimum at 216 nm and a strong positive band at 195 nm is not indicative of a model β-sheet structure either. The observed negative band at 200 nm would rather be characteristic of an unfolded/random coil protein. This is however not inconsistent with the NMR results since the existence of all β-proteins whose CD spectra resemble the spectra of unordered proteins is well documented, and for some of them it has been shown that their

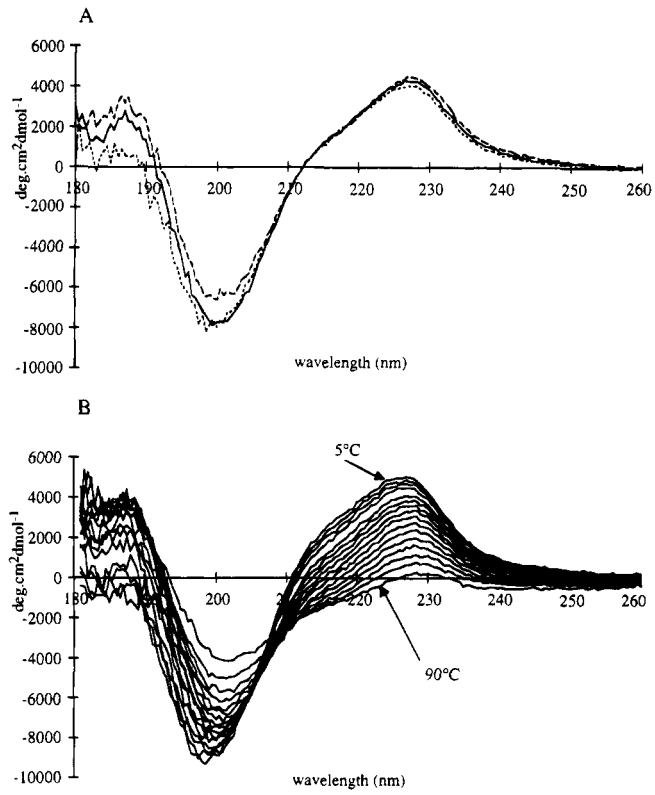

FIGURE 10: (A) Circular dichroism spectra of PMP-D2 in water pH 6.6 (- - -), in the presence of 27% trifluoroethanol (—), and in the presence of 27% acetonitrile (— —). The concentration of PMP-D2 was 5.8 × 10^{-5} M. (B) Circular dichroism spectra of PMP-D2 when increasing temperature from 5 to 90 °C. PMP-D2 was dissolved in water at a concentration of 5.8 × 10^{-5} M.

β-sheets are either distorted or form short irregular β-strands (Wu *et al.*, 1992). However, in contrast to these compact and rigid proteins, which usually show a sharp transition upon thermal denaturation, the CD spectrum of PMP-D2 changed linearly when increasing the temperature (Figure 10B), suggesting that the unfolding was not a cooperative process. In addition, when increasing the temperature, the whole spectrum was modified uniformly at 200 and 227 nm, indicating that there is no local resistance to environment changes. The broad positive band at 227 nm can be assigned most probably to the Trp-25 side chain (Woody, 1978; Ménez *et al.*, 1976). Although there is only one aromatic residue, the magnitude of this effect is strong and might be due to either its environment (i.e., the interaction with Lys-10 as shown in the NMR structure) or to the rigid conforma-

tion of the Trp residue which might furthermore enhance the ellipticity of this aromatic chromophore. A remarkable feature of the CD spectrum of PMP-D2 is that, even when increasing the ionic strength or when in the presence of an organic solvent such as trifluoroethanol or acetonitrile, no significant changes could be observed. This suggests a highly rigid structure of PMP-D2, which is consistent with the identification of hydrophobic clusters (see above). A similar conservation of the structure in the presence of trifluoroethanol has also been reported for another peptide with a high cysteine content, i.e., α-neurotoxin (Ménez *et al.*, 1976).

Comparison with ω-Conotoxin GVIA

Since PMP-D2 is a small peptide with a high disulfide content, we have compared its sequence to small toxins from the SWISS-PROT (Bairoch *et al.*, 1991) and PIR (Sidman *et al.*, 1988) databases; however, no similarities or consensus sequence could be found. Nevertheless, functional and structural considerations lead to comparison of PMP-D2 with ω-conotoxin GVIA, a neuronal voltage-sensitive Ca^{2+} channel blocker (Olivera *et al.*, 1984; McCleskey *et al.*, 1987). Preliminary electrophysiology experiments show that PMP-D2 inhibits mammalian Ca^{2+}-dependent currents at concentrations ranging between 0.1 and 10 μM (Harding *et al.*, 1994). Qualitative comparison of PMP-D2 structure determined here to the recently published solution structure of ω-conotoxin GVIA (Davis *et al.*, 1993; Sevilla *et al.*, 1993; Pallaghy *et al.*, 1993) shows that some similarities exist between the two molecules; ω-conotoxin is a 27 amino acid peptide which contains three disulfide bridges, and PMP-D2 is a 35 amino acid peptide containing three disulfide bridges. Although ω-conotoxin does not have the same disulfide pattern as PMP-D2, both molecules contain a small three-stranded antiparallel β-sheet involving residues 6−8, 18−21, and 24−27 for ω-conotoxin and residues 8−11, 15−19, and 25−29 for PMP-D2. It should be noted however that the connections between the strands differ in the two molecules, and thus the overall topologies are different. More interestingly, most of the hydrophilic amino acid side chains located on the accessible face of the β-sheet contain hydroxyl groups; Thr-16, Thr-18, Thr-20, and Thr-28 for PMP-D2 and Ser-18, Tyr-22, Thr-23, and Tyr-27 for ω-conotoxin. In both molecules, the four amino acids preceding the first strand of the β-sheet form a type II β-turn with a proline or an hydroxyproline in position 2 of the turn (Pro-6 in PMP-D2 and Hyp-4 in ω-conotoxin) and a glycine in position 3 of the turn. This glycine is conserved in all known ω-conotoxins (Hillyard *et al.*, 1989; Gray *et al.*, 1988), implying that the turn may also be conserved among ω-conotoxins.

In view of the structural and functional similarities between the two molecules, we suggest that both molecules would bind to the Ca^{2+} channels in a similar way. Although various attempts have been made in order to evaluate which amino acids, particularly among the basic amino acids, are critical for the binding of ω-conotoxin (Sato *et al.*, 1993; Lampe *et al.*, 1993), no conclusive results have been obtained. From the comparison of the three-dimensional structures of PMP-D2 and ω-conotoxin, we propose that the hydroxyl groups of Thr-16, Thr-18, Thr-20, and Thr-28 in PMP-D2 and the hydroxyl groups of Ser-18, Tyr-22, Thr-23, and Tyr-27 in ω-conotoxin, which are all exposed on the outside surface of the β-sheet, might be essential for the binding to the Ca^{2+} channels. This hypothesis can be tested by preparing protein variants of PMP-D2 in which those amino acids are replaced by nonhydroxylated side-chain amino acids.

CONCLUSIONS

Based on NMR data, we have shown that in solution PMP-D2 adopts a compact globular fold which forms a cavity demarcated by a small three-stranded β-sheet. This fold is stabilized by three disulfide bridges (Cys4−Cys19, Cys14−Cys32, and Cys17−Cys27) that have been assigned from NMR data and structure calculations and independently confirmed using chemical and enzymatic methods. Hydrophobic clusters are also involved in the stabilization of the tertiary structure: Trp-25, Cys-4, Cys-17, Cys-19, and Cys-27 inside the cavity and Val-9/Thr-18, Thr16/Thr-28, and Thr-20/Val-24 on the convex side of the β-sheet.

From comparison with the three-dimensional structure of ω-conotoxin GVIA, we have proposed that the hydroxyl groups located on the accessible face of the β-sheet would be involved in the binding of PMP-D2 to the Ca^{2+} channels.

It was previously reported that PMP-D2 acts as a serine proteinase inhibitor (Boigegrain *et al.*, 1992); however, the sequence of PMP-D2 is not related to any currently characterized class of serine proteinase inhibitors (Laskowski & Kato, 1980). With the recent publications of the NMR structure of *Ascaris* trypsin inhibitor (ATI) (Grasberger *et al.*, 1994) and the crystal structure of *Ascaris* chymotrypsin/elastase inhibitor (C/E-1) complexed with elastase (Huang *et al.*, 1994), one can compare the structure of PMP-D2 to two inhibitors that are homologous to PMP-D2 with respect to the pattern of disulfide bridges. These two proteins are composed of 62 and 63 amino acids, respectively, and each contain five disulfide bridges. Two of the disulfide bridges, Cys15−Cys33 and Cys18−Cys29 for ATI and Cys14−Cys33 and Cys17−Cys29 for C/E-1, are homologous to the disulfide bridges Cys14−Cys32 and Cys17−Cys27 of PMP-D2. In ATI and C/E-1, these two sets of disulfide bridges stabilize the reactive site, which is located between residues Cys-29 and Cys-33. The disulfide bridges Cys18−Cys29 of ATI and Cys17−Cys29 of C/E-1 delimit the ends of a loop which range from residues 19 and 18 for ATI and C/E-1, respectively, to residue 28; there is a turn between residues 20 and 24 in ATI. In PMP-D2, the corresponding segment has a hairpin structure which contains the second and third strands of the small β-sheet, which are connected by a turn between residues 20 and 24.

To conclude, it should be mentioned that Schweitz *et al.* (1994) have described a 60 amino acid peptide from the venom of the oriental green mamba *Dendroaspis angusticeps* that belongs to the superfamily of Kunitz-type trypsin inhibitors and that is a potent blocker of high-threshold Ca^{2+} channels. Thus, further studies with PMP-D2 are currently in progress to evaluate its potential inhibiting effect on various serine proteinases as well as to characterize its effect on Ca^{2+} channels.

ACKNOWLEDGMENT

We are grateful to Dr. Bruno Kieffer for his advice in structure calculations and for helpful discussions. CD spectra were recorded at Marion Merell Dow Research Institute, Strasbourg (France), and we express our gratitude to Dr. J. T. Pelton and C. Brokel for valuable discussions and their help with the CD experiments.

REFERENCES

Adler, M., Carter, P., Lazarus, R. A., & Wagner, G. (1993) *Biochemistry 32*, 282−289.

Bairoch, A., & Boekmann, B. (1993) *Nucleic Acids Res. 21*, 3093−3096.

Banks, K. M., Hare, D. R., & Reid, B. R. (1989) *Biochemistry 28*, 6996−7010.

Bax, A., & Davis, D. G. (1985) *J. Magn. Reson. 65*, 355−359.

Bystrov, V. F. (1976) *Prog. Nucl. Magn. Reson. Spectrosc. 10*, 41−82.

Boigegrain, R.-A., Mattras, H., Brehélin, M., Paroutaud, P., & Coletti-Previero, M.-A. (1992) *Biochem. Biophys. Res. Commun. 189*, 790−793.

Braunschweiler, L. R., & Ernst, R. R. (1983) *J. Magn. Reson. 53*, 521−528.

Brooks, B. R., Bruccoleri, R. E., Olafson, B. D., States, D. J., Swaminathan, S., & Karplus, M. (1983) *J. Comput. Chem. 4*, 187−217.

Brünger, A. T. (1992) *X-PLOR Manual, V3.0*, Yale University, New Haven, CT.

Davis, J. H., Bradley, E. K., Mijanich, G. P., Nadasdi, L., Ramachandran, J., & Basus, V. J. (1993) *Biochemistry 32*, 7396−7405.

Dill, K. A., Fiebig, K. M., & Chan, H. S. (1993) *Proc. Natl. Acad. Sci. U.S.A. 90*, 1942−1946.

Grasberger, B. L., Clore, G. M., & Gronenborn, A. M. (1994) *Structure 2*, 669−678.

Gray, W. R. (1993a) *Protein Sci. 2*, 1732−1748.

Gray, W. R. (1993b) *Protein Sci. 2*, 1749−1755.

Gray, W. R., Olivera, B. M., & Cruz, L. J. (1988) *Annu. Rev. Biochem. 57*, 665−700.

Harding, L., Scott, R. H., Kellenberger, C., Hietter, H., Luu, B., Beadle, D. J., & Bermudez, I. (1994) *J. Recept. Res.* (in press).

Hietter, H., Luu, B., Goltzene, F., Zachary, D., Hoffmann, J., & Van Dorsselaer, A. (1989) *Eur. J. Biochem. 82*, 77−84.

Hietter, H., Van Dorsselaer, A., Green, B., Denoroy, L., Hoffmann, J., & Luu, B. (1990) *Eur. J. Biochem. 187*, 241−247.

Hietter, H., Van Dorsselaer, A., & Luu, B. (1991) *Insect Biochem. 21*, 259−264.

Hillyard, D. R., Olivera, B. M., Woodward, S., Corpuz, G. P., Gray, W. R., Ramilo, C. A., & Cruz, L. J. (1989) *Biochemistry 28*, 358−361.

Huang, K., Strynadka, N. C. J., Bernard, V. D., Peanasky, R. J., & James, M. N. G. (1994) *Structure 2*, 679−689.

Jaquinod, M., Potier, N., Klarskov, K., Reymann, J. M., Sorokine, O., Kieffer, S., Barth, P., Andriantomanga, V., Biellmann, J.-F., & Van Dorsselaer, A. (1993) *Eur. J. Biochem. 218*, 893−903.

Jeener, J., Meier, B. H., Bachmann, P., & Ernst, R. R. (1979) *J. Chem. Phys. 71*, 4546−4553.

Karplus, M. (1959) *J. Chem. Phys. 30*, 11−15.

Kellenberger, C., Hietter, H., Trifilieff, E., & Luu, B. (1994) in *Innovation and Perspectives in Solid Phase synthesis* (Epton, R., Ed.) Mayflower World Wide Ltd., CH102, 567−570.

Koehl, P., Lefèvre, J.-F., & Jardetzky, O. (1992) *J. Mol. Biol. 223*, 299−315.

Kraulis, P. J. (1991) *J. Appl. Crystallogr. 24*, 946−950.

Kumar, A., Ernst, R. R., & Wüthrich, K. (1980) *Biochem. Biophys. Res. Commun. 95*, 1−6.

Laskowski, M., & Kato, I. (1980) *Annu. Rev. Biochem. 49*, 593−626.

Lampe, R. A., Lo, M. M. S., Keith, R. A., Horn, M. B., McLane, M. W., Herman, J. L., & Spreen, R. C. (1993) *Biochemistry 32*, 3255−3260.

Marion, D., & Wüthrich, K. (1983) *Biochem. Biophys. Res. Commun. 113*, 967.

McCleskey, E. W., Fox, A. P., Feldman, D. H., Cruz, L. J., Olivera, B. M., Tsien, R. W., & Yoshikami, D. (1987) *Proc. Natl. Acad. Sci. U.S.A. 84*, 4327−4331.

Ménez, A., Bouet, F., Tamiya, N., & Fromageot, P. (1976) *Biochim. Biophys. Acta 453*, 121−132.

Montelione, G. T., Arnold, E., Meinwald, Y. C., Stimson, E. R., Denton, J. B., Huang, S.-G., Clardy, J., & Scheraga, H. A. (1984) *J. Am. Chem. Soc. 106*, 7946−7958.

Morris, A. L., MacArthur, M. W., Hutchinson, E. G., & Thornton, J. M. (1992) *Proteins 12*, 345−364.

Nakakura, N., Hietter, H., Van Dorsselaer, A., & Luu, B. (1992) *Eur. J. Biochem. 204*, 147−153.

Olivera, B. M., McIntoch, J. M., Cruz, L. J., Luque, F. A., & Gray, W. R. (1984) *Biochemistry 23*, 5087−5090.

Pallaghy, P. K., Duggan, B. M., Pennington, M. W., & Norton, R. S. (1993) *J. Mol. Biol. 234*, 405−420.

Pardi, A., Billeter, M., & Wüthrich, K. (1984) *J. Mol. Biol. 180*, 741−751.

Rance, M., Sorensen, O. W., Bodenhausen, G., Wagner, G., Ernst, R. R., & Wüthrich, K. (1983) *Biochem. Biophys. Res. Comm. 117*, 479.

Richardson, J. S. (1981) *Adv. Protein Chem. 34*, 167−339.

Sato, K., Park, N.-G., Kohno, T., Maeda, T., Kim, J., II, Kato, R., & Takahashi, M. (1993) *Biochem. Biophys. Res. Commun. 194*, 1292−1296.

Schweitz, H., Heurteauz, C., Bois, P., Moinier, D., Romey, G., & Lazdunski, M. (1994) *Proc. Natl. Acad. Sci. U.S.A. 91*, 878−882.

Sevilla, P., Bruix, M., Santoro, J., Gago, F., Garcia, A. G., & Rico, M. (1993) *Biochem. Biophys. Res. Commun. 192*, 1238−1244.

Sidman, K. E., George, D. G., Barker, W. C., & Hunt, L. T. (1988) *Nucleic Acids Res. 11*, 1869−1871.

Thornton, J. M. (1981) *J. Mol. Biol. 151*, 261−287.

Wagner, G., Braun, W., Havel, T. F., Schaumann, T., Go, N., & Wüthrich, K. (1987) *J. Mol. Biol. 196*, 611−638.

Wishart, D. S., Sykes, B. D., & Richards, F. M. (1992) *Biochemistry 31*, 1647−1651.

Woody, R. W. (1978) *Biopolymers 17*, 1451−1467.

Wu, J., Yang, J. T., & Wu, C.-S. C. (1992) *Anal. Biochem. 200*, 359−364.

Wüthrich, K. (1986) *NMR of Proteins and Nucleic Acids*; John Wiley & Sons, New York.

Yoshikami, D. (1987) *Proc. Natl. Acad. Sci. U.S.A. 84*, 4327−4331.